Combined Methodology for Analysis of Rotary Systems

Yuan Mao Huang
Professor
e-mail: ymhuang@ccms.ntu.edu.tw

Chin-Ming Wang
Research Assistant

Department of Mechanical Engineering,
National Taiwan University,
Taipei, Taiwan
Republic of China

This study develops a numerical method for analyzing the unbalanced effect of rotary systems by combining the finite element method, the transfer matrix method, the time marching numerical integration method and the Houbolt numerical method. Previous studies of the individual effects associated with the rotary inertia, gyroscopic phenomenon, shear deformation, axial loading and internal damping on the dynamic behavior of rotary systems are all incorporated and examined in this study. The calculated transient and steady displacements of components in two systems are comparable with the available data. The results show that maximum displacements occur in the transient states at some critical speeds to assure the importance for analyzing the unbalanced effect of the rotary systems. Compared with existing methods, this presently combined methodology provides a faster converging speed. In addition, this model should improve the predicted results for the transient dynamic analysis of rotary systems than those obtained from existing models. [DOI: 10.1115/1.1385204]

Introduction

Steady state responses are investigated in most analyses of dynamic rotary systems. While the transient dynamic characteristics of the system before reaching the steady state are important, they are complicated. The transient dynamic behavior of the system has a significant effect on the steady state response of the system, especially when it operates near the critical speed or with an unbalanced force generated.

Adams [1] used the Jeffcott rotor formulation and Nelson [2] used the finite element method to develop models for rotary systems. Dokainish [3] combined the finite element method and the transfer matrix method [4] to reduce the size of the global matrix. Kumar and Sankar [5] developed the discrete time transfer matrix method. Subbiah et al. [6] simulated the model with the Nelson and McVaugh's finite element model [7] to develop a new transient property transfer approach. The finite element method is an effective technique for the transient analysis. However, the degrees of freedom and the required computer memory increase significantly when the number of elements increases. Therefore, there may be a loss in efficiency for large rotor systems. To improve the efficiency for analyzing the dynamic behavior of a rotary system, the present study developed a numerical method by combining the finite element method, the transfer matrix method, the time marching numerical integration method and the Houbolt numerical method [8]. Furthermore, individual effects due to the rotary inertia, gyroscopic phenomenon, shear deformation, axial load and internal damping on the transient response of the system that have been analyzed by Nelson [2], Dokainish [3], Subbiah et al. [6], Nelson and McVaugh [7], Özguven and Özkan [9], Subbiah and Rieger [10], and Alam and Nelson [11] were all incorporated in the present study. It was hypothesized that this proposed methodology would improve calculated results with a faster converging speed than existing methods and models, especially, for large rotary systems.

Finite Element Model of Components

A finite element as shown in Fig. 1 has eight degrees of freedom, q_i, $i=1,2,3,\ldots 8$. There are two translational displacements and two rotational displacements for each end. The approximated translational displacement and rotational displacement at any point in the element of the shaft can be expressed, respectively, by

$$\begin{Bmatrix} y(s,t) \\ z(s,t) \end{Bmatrix} = \begin{bmatrix} \psi_1 & 0 & 0 & \psi_2 & \psi_3 & 0 & 0 & \psi_4 \\ 0 & \psi_1 & -\psi_2 & 0 & 0 & \psi_3 & -\psi_4 & 0 \end{bmatrix} \{\mathbf{q}(t)\} \tag{1}$$

$$\begin{Bmatrix} \theta_y(s,t) \\ \theta_z(s,t) \end{Bmatrix} = \begin{bmatrix} 0 & -\phi_1 & \phi_2 & 0 & 0 & -\phi_3 & \phi_4 & 0 \\ \phi_1 & 0 & 0 & \phi_2 & \phi_3 & 0 & 0 & \phi_4 \end{bmatrix} \times \{\mathbf{q}(t)\} \tag{2}$$

where the distance s is measured from the left end of the point of interest [7]. The symbol $\{\mathbf{q}(t)\}$ is the displacement vectors of nodal points at both ends of the element. The shape functions $\psi_j(s)$ and $\phi_k(s)$ are the static displacement modes when one end has a unit displacement and another end has zero displacement. Both shape functions are functions of the location, geometry and material properties. The centroid locations of the cross sections in elements are assumed to be a linear distribution.

Considering all of the effects of the rotary inertia, gyroscopic effect, axial loading, shear deformation and internal damping, and substituting kinetic energy, the potential energy and the virtual work due to the unbalanced force into the Hamilton's equation yields

$$([M_T^s]+[M_R^s])\{\ddot{\mathbf{q}}^s\}+(\eta_V[K_B^s]-\Omega[G^s])\{\dot{\mathbf{q}}^s\}+\left[\frac{1+\eta_H}{\sqrt{1+\eta_H^2}}[K_B^s] -[K_A^s]+\left(\eta_V\Omega+\frac{\eta_H}{\sqrt{1+\eta_H^2}}\right)[K_C^s]\right]\{\mathbf{q}^s\}=\{F^s\} \tag{3}$$

where the coefficient matrix $[M_T^s]$ is the function of the mass, length and transverse shear effect, the coefficient matrices $[M_R^s]$ and $[G^s]$ are the function of the mass, diameter, length and transverse shear effect, the coefficient matrices $[K_B^s]$, $[K_A^s]$ and $[K_C^s]$ are the function of the transverse shear effect and axial loading, and the unbalanced force in an element can be expressed as

$$\{F^s\}=\{F_c^s\}\cos\Omega t+\{F_s^s\}\sin\Omega t \tag{4}$$

where

Contributed by the Technical Committee on Vibration and Sound for publication in the JOURNAL OF VIBRATION AND ACOUSTICS. Manuscript received Nov. 1999; revised Jan. 2001. Associate Editor: C. Pierre.

 Copyright © 2001 by ASME

Downloaded 03 Nov 2008 to 140.112.113.225. Redistribution subject to ASME license or copyright; see http://www.asme.org/terms/Terms_Use.cfm

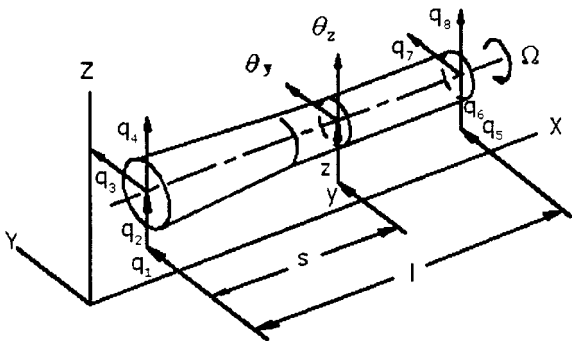

Fig. 1 Coordinates of element

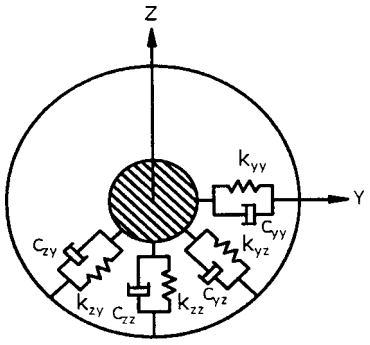

Fig. 2 Bearing model

$$\{F_c^s\}=\int_0^l m[\Psi]^T\begin{bmatrix}\Omega^2 & \dot{\Omega}\\ -\dot{\Omega} & \Omega^2\end{bmatrix}\begin{Bmatrix}y\\ z\end{Bmatrix}ds$$

$$\{F_s^s\}=\int_0^l m[\Psi]^T\begin{bmatrix}\dot{\Omega} & -\Omega^2\\ \Omega^2 & \dot{\Omega}\end{bmatrix}\begin{Bmatrix}y\\ z\end{Bmatrix}ds \tag{5}$$

The matrix of the gyroscopic effect is skew symmetric, and the other coefficient matrices are symmetric.

Similarly, considering the disk as a point mass with four degrees of freedom and applying the Hamilton principle, the resulting equation is

$$([M_T^d]+[M_R^d])\{\ddot{\mathbf{q}}^d\}-\Omega[G^d]\{\dot{\mathbf{q}}^d\}=\{F^d\} \tag{6}$$

where $[M_T^d]$, $[M_R^d]$ and $[G^d]$ are matrices of m^d, I_D^d and I_P^d, respectively [7]. The unbalanced force of the disk is

$$\{F_D\}=\{F_c^d\}\cos\Omega t+\{F_s^d\}\sin\Omega t+\{F_g\} \tag{7}$$

where

$$\{F_c^d\}=m^d\begin{bmatrix}\Omega^2 & \dot{\Omega} & 0 & 0\\ -\dot{\Omega} & \Omega^2 & 0 & 0\\ 0 & 0 & 0 & 0\\ 0 & 0 & 0 & 0\end{bmatrix}\begin{Bmatrix}y^d\\ z^d\\ 0\\ 0\end{Bmatrix}$$

$$\{F_s^d\}=m^d\begin{bmatrix}\dot{\Omega} & -\Omega^2 & 0 & 0\\ \Omega^2 & \dot{\Omega}^2 & 0 & 0\\ 0 & 0 & 0 & 0\\ 0 & 0 & 0 & 0\end{bmatrix}\begin{Bmatrix}y^d\\ z^d\\ 0\\ 0\end{Bmatrix} \tag{8}$$

$$\{F_g\}=\begin{Bmatrix}0\\ -m^dg\\ 0\\ 0\end{Bmatrix}$$

The bearing is assumed to consist of four springs and four dampers as shown in Fig. 2, and the load acting on the bearing concentrated at the node is [9]

$$\{F^b\}=-[C^b]\{\dot{\mathbf{q}}^b\}-[K^b]\{\mathbf{q}^b\} \tag{9}$$

where

$$\{\mathbf{q}^b\}=\begin{Bmatrix}y\\ z\end{Bmatrix}$$

$$[C^b]=\begin{bmatrix}c_{yy} & c_{yz}\\ c_{zy} & c_{zz}\end{bmatrix}$$

$$[K^b]=\begin{bmatrix}k_{yy} & k_{yz}\\ k_{zy} & k_{zz}\end{bmatrix} \tag{10}$$

From the Newmark method [12], the Wilson method [13] and the Houbolt method [8], the angular acceleration and the angular velocity can be expressed, respectively, as

$$\{\ddot{\mathbf{q}}(t_i)\}=A(t_i)\{\mathbf{q}(t_i)\}+\{B(t_i)\} \tag{11}$$

and

$$\{\dot{\mathbf{q}}(t_i)\}=D(t_i)\{\mathbf{q}(t_i)\}+\{E(t_i)\} \tag{12}$$

where the coefficients $A(t_i)$, $D(t_i)$, $\{B(t_1)\}$ and $\{E(t_i)\}$ depend on the numerical integration used.

The force between the $(n-1)$th and the nth elements in the shaft is shown in Fig. 3. If the external load acting on the nth nodal point is $\{F_n(t_i)\}$, the loads acting on the right side of the $(n-1)$th element and the left side of the nth element are $\{f_n^L(t_i)\}$ and $\{f_n^R(t_i)\}$, respectively. The static balance equation is [14]

$$\{f_n^R(t_i)\}=\{F_n(t_i)\}-\{f_n^L(t_i)\} \tag{13}$$

Substituting Eqs. (11), (12) and (13) into Eq. (3) yields

$$\{\mathbf{u}_{n+1}^L(t_i)\}=[T_n^s(t_i)]\{\mathbf{u}_n^L(t_i)\} \tag{14}$$

where $\{\mathbf{u}_{n+1}^L\}$ and $\{\mathbf{u}_n^L\}$ are the state vectors of the right sides of the nth and the $(n-1)$th elements, and $[T_n^s]$ is the transfer matrix.

The nth nodal point for the disk between two shaft elements is shown in Fig. 4. The external load $\{F_n^d\}$ that is the resultant interaction force between elements and the unbalanced force of the disk is

$$\{F_n^d(t_i)\}=-\{f_n^L(t_i)\}-\{f_n^R(t_i)\}+\{F_D(t_i)\} \tag{15}$$

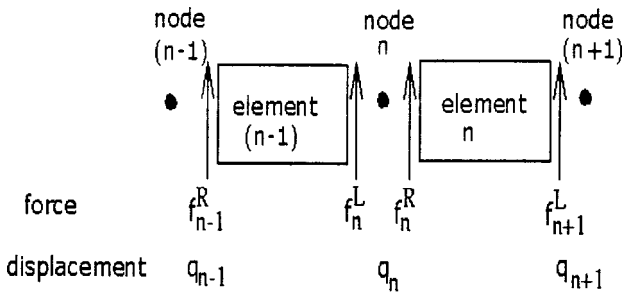

Fig. 3 Force between two elements

Downloaded 03 Nov 2008 to 140.112.113.225. Redistribution subject to ASME license or copyright; see http://www.asme.org/terms/Terms_Use.cfm

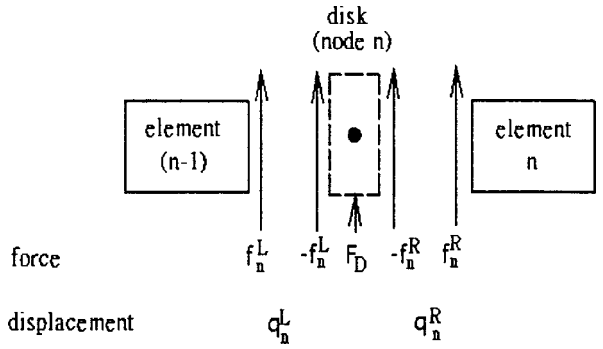

Fig. 4 Force between disk and shaft

Substituting Eqs. (11), (12) and (15) into Eq. (6) with the consistent property of the nodal point

$$\{\mathbf{q}_n^L\}=\{\mathbf{q}_n^R\} \tag{16}$$

yields

$$\{\mathbf{u}_n^R(t_i)\}=[T_n^d(t_i)]\{\mathbf{u}_n^L(t_i)\} \tag{17}$$

where $\{\mathbf{u}_n^R\}$ and $\{\mathbf{u}_n^L\}$ are the state vectors on the left side of the nth element and the right side of the $(n-1)$th element, and $[T_n^d]$ is the transfer matrix.

The bearing between two elements of the shaft can be considered as a point element as shown in Fig. 5. The equation of force balance of the bearing is

$$\{F^b(t_i)\}=\{f_n^L(t_i)\}+\{f_n^R(t_i)\} \tag{18}$$

Substituting Eqs. (9), (16) and (18) into the equation of motion, the relationship of state vectors can be expressed as

$$\{\mathbf{u}_n^R(t_i)\}=[T_n^b(t_i)]\{\mathbf{u}_n^L(t_i)\} \tag{19}$$

where $\{\mathbf{u}_n^R\}$ and $\{\mathbf{u}_n^L\}$ are the state vectors of the left side of the nth element and the right side of the $(n-1)$th element, and $[T_n^b]$ is the transfer matrix of the bearing. Applying the transfer matrix method, the relationship of state vectors for both ends of the system can be expressed as

$$\{\mathbf{u}_m^R(t_i)\}=[T_m(t_i)][T_{m-1}(t_i)]\cdots[T_2(t_i)][T_1(t_i)]\{\mathbf{u}_1^L(t_i)\}$$
$$=[T_{sys}(t_i)]\{\mathbf{u}_l^L(t_i)\} \tag{20}$$

where $[T_{sys}]$ stands for the overall transfer matrix [4]. Using the Houbolt numerical integration method with the appropriate boundary condition and the quantities obtained from the previous time step as the initial condition, $\{\mathbf{u}_m^R(t_i)\}$, $\{\mathbf{u}_l^L(t_i)\}$ and the state vector at any location can be determined [8].

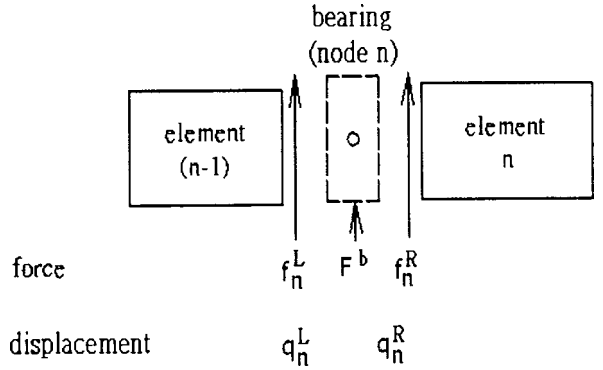

Fig. 5 Force between bearing and shaft

Result

The first system analyzed is illustrated in Fig. 6 and consists of a disk at the center of a shaft that is supported by two identical nonisotropic bearings at each end. The mass of the disk is assumed to be concentrated at a point with an eccentricity from the disk center due to unbalance at time $t=0$. Each bearing is simulated by four springs and four dampers. The shaft is assumed to be uniform and flexible. The data for the system used in the analysis is obtained from Subbiah and Rieger [10] and shown in Table 1.

The shaft is divided into eight identical elements. There are a total of 36 degrees of freedom for the system. The boundary condition has no load acting on either end of the shaft. The system is considered to be undamped at time $t=0$, and the resulting displacements are then used as the starting values for the subsequent iteration of the damped system [10]. When the rotational speed is 40 rev/s, the system reaches the steady state within the third revolution. The effects of the step number for each revolution, N_C, on the accuracy of result and the converging speed are studied. The maximum deviations between the calculated transient displacements and the data obtained by Subbiah and Rieger [10] for various N_C are shown in Table 2. The value of N_C equal to 30 is used for further analysis. The calculated transient and steady displacements of the disk center and the data obtained by Subbiah and Rieger [10] are shown in Figs. 7 and 8, respectively. The symbols y and z are the displacements in the Y and Z directions, respec-

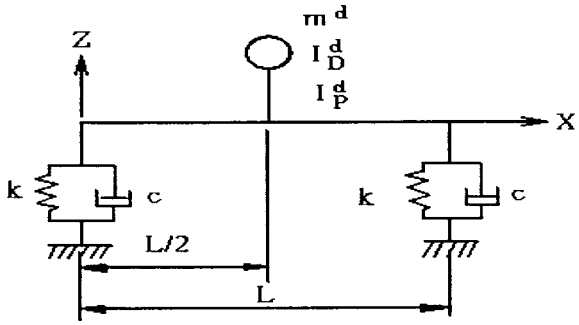

Fig. 6 Rotary system

Table 1 Data of first system

mass of disk m^d	566 kg
eccentricity of disk	1.766×10^{-8} m
length of shaft l	0.437 m
diameter of shaft d^S	0.091 m
density of shaft ρ	0.775×10^4 kg/m^3
Young's modulus of shaft E	0.2×10^{12} N/m^2
stiffness of shaft k_{yy}	11.4×10^7 N/m
k_{yz}	0.1×10^7 N/m
k_{zy}	0.1×10^7 N/m
K_{zz}	7.2×10^7 N/m
damping coefficient of bearing c_{yy}	5.9×10^5 N.s/m
c_{yz}	0.1×10^5 N.s/m
c_{zy}	0.1×10^5 N.s/m
c_{zz}	1.7×10^5 N.s/m

Table 2 Effect of N_C on deviation of maximum transient displacement

N_C	20	25	30	35	40
deviation	7.14%	3.57%	2.86%	2.23%	2.07%

Downloaded 03 Nov 2008 to 140.112.113.225. Redistribution subject to ASME license or copyright; see http://www.asme.org/terms/Terms_Use.cfm

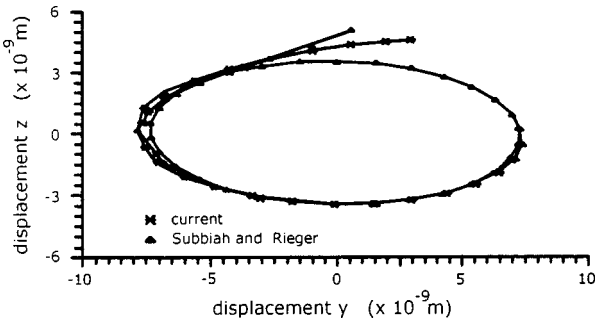

Fig. 7 Transient displacement of disk center with $N_C=30$

tively. The calculated transient displacements of the centers at the disk and bearings are shown in Fig. 9. The time required for a rotary system to reach the steady state varies for different rotational speeds. The maximum transient displacements at the disk center versus the rotational speed of the shaft calculated in this study, obtained from Subbiah and Rieger [10] and obtained from the software ANSYS are shown in Fig. 10. Similarly, the calculated maximum transient displacement of the bearing center versus the rotational speed of the shaft is shown in Fig. 11.

The second system used in the analysis that is similar to the system as shown in Fig. 6 is an asymmetric system. The disk is at a distance that is at the four fifth of the shaft length measured from the left end of the shaft and the bearings are orthotropic. The data of this asymmetric system obtained from Alam and Nelson [11] who analyzed the steady state and transient state by using the component mode synthesis are shown in Table 3.

Both ends of the shaft are free and the shaft is divided into five elements. With the disk as a point element there are twenty four degrees of freedom for the system. The calculated maximum transient displacements in the *Y* and *Z* directions versus the rotational speed of the shaft and the data obtained by Alam and Nelson [11] are shown in Figs. 12 and 13, respectively. The maximum steady

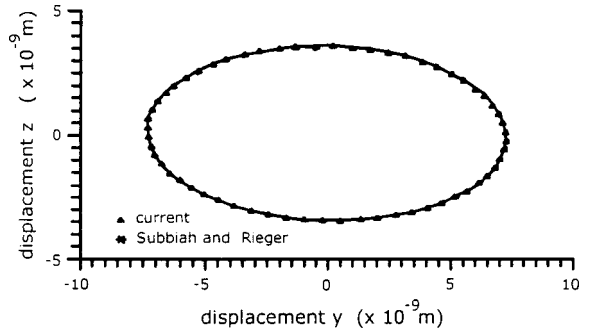

Fig. 8 Steady displacement of disk center with $N_C=30$

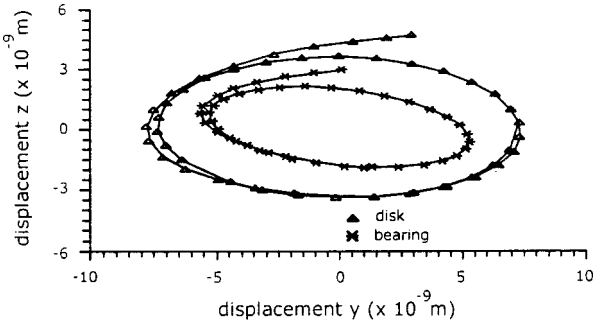

Fig. 9 Transient displacements of centers at disk and bearings with $N_C=30$

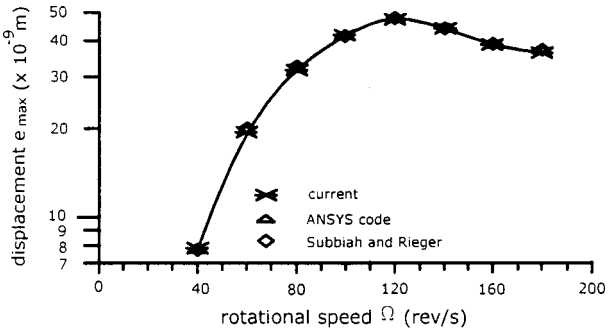

Fig. 10 Maximum transient displacement of disk center versus rotational speed with $N_C=30$

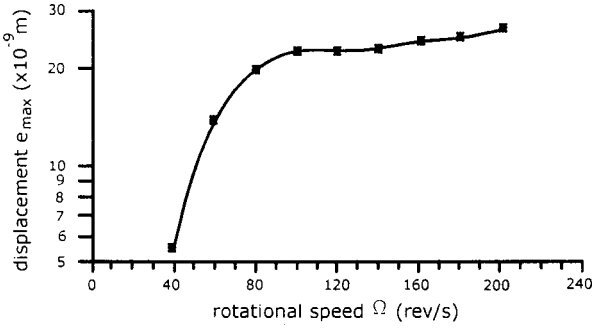

Fig. 11 Maximum transient displacement of bearing center versus rotational speed with $N_C=30$

Table 3 Data of second system

mass of disk m^d		4.9035 kg
disk diametral mass moment of inertia I_D^d		0.01356 kg.m^2
disk polar moment of inertia I_P^d		0.02712 kg.m^2
eccentricity of disk		0.254 mm
length of disk L		0.508 m
diameter of shaft d^s		0.0508 m
density of shaft ρ		8304 kg/m^3
Young's modulus of shaft E		20.69 x 10^{10} N/m^2
stiffness of bearing	K_{yy}	0.437815 x 10^8 N/m
	K_{yz}	0
	K_{zy}	0
	K_{zz}	2.62689 x 10^8 N/m
damping coefficient of bearing	c_{yy}	876 N.s/m
	c_{yz}	0
	c_{zy}	0
	c_{zz}	525 N.s/m

displacements of the disk center in the *Y* and *Z* directions versus the rotational speed and the data obtained by Alam and Nelson [11] are shown in Figs. 14 and 15, respectively. When the rotational speed of the shaft is 1550 rad/s, with N_C equal to 30 the transient displacement of the disk center is shown in Fig. 16. The system reaches the steady state within 45 revolutions, and the steady displacement of the disk center is shown in Fig. 17. The maximum displacement occurs at 0.2036 s. If the rotational speed of the shaft is 3100 rad/s, the transient displacement of the disk center with N_C equal to 30 is shown in Fig. 18. The steady displacement of the disk center that reaches the steady state within 80 revolutions is shown in Fig. 19. The maximum displacement

Downloaded 03 Nov 2008 to 140.112.113.225. Redistribution subject to ASME license or copyright; see http://www.asme.org/terms/Terms_Use.cfm

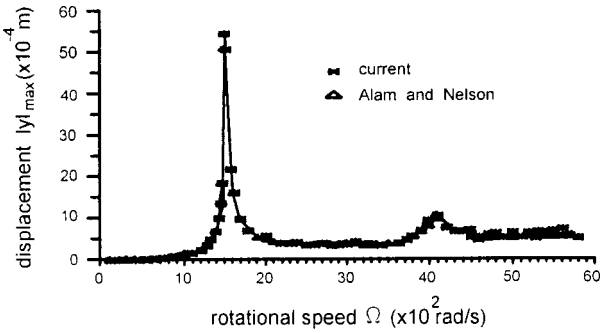

Fig. 12 Maximum transient displacement of disk center in *Y* direction versus rotational speed

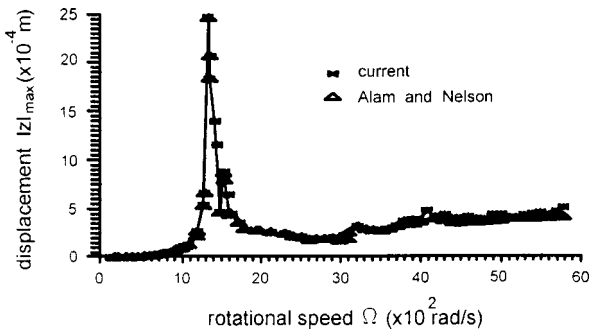

Fig. 13 Maximum transient displacement of disk center in *Z* direction versus rotational speed

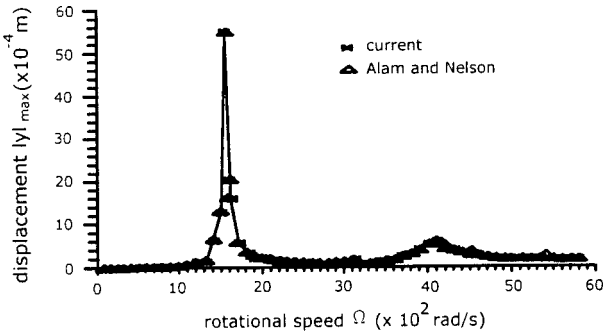

Fig. 14 Maximum steady displacement of disk center in *Y* direction versus rotational speed

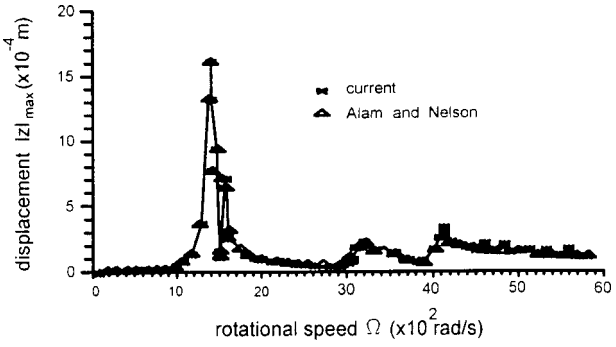

Fig. 15 Maximum steady displacement of disk center in *Z* direction versus rotational speed

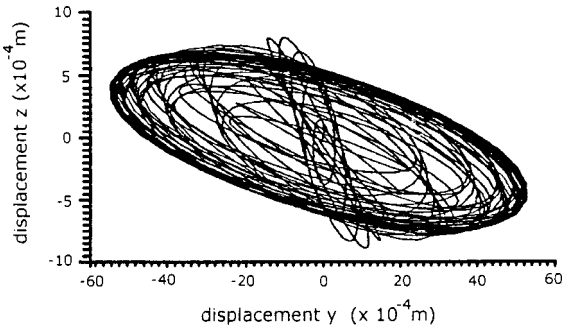

Fig. 16 Transient displacement trace of disk center at $\Omega = 1550$ rad/s

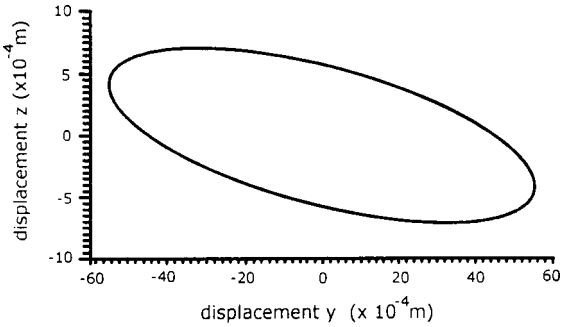

Fig. 17 Steady displacement trace of disk center at $\Omega = 1550$ rad/s

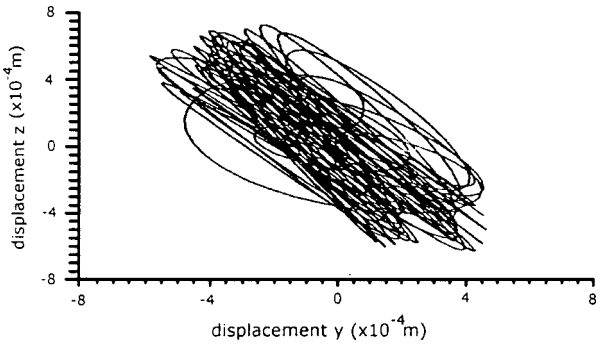

Fig. 18 Transient displacement of disk center at $\Omega = 3100$ rad/s

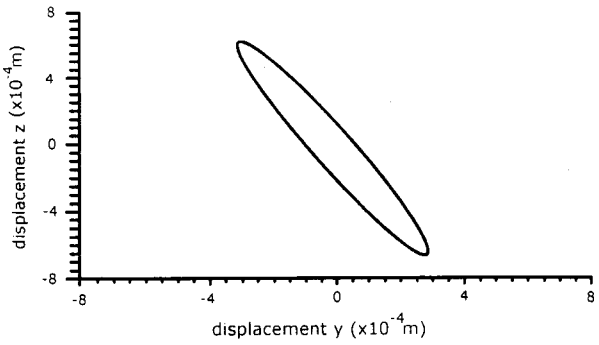

Fig. 19 Steady displacement of disk center at $\Omega = 3100$ rad/s

Downloaded 03 Nov 2008 to 140.112.113.225. Redistribution subject to ASME license or copyright; see http://www.asme.org/terms/Terms_Use.cfm

occurs at 0.0162 s. If the rotational speed of the shaft is 4100 rad/s, with N_C equal to 40, then the system reaches the steady state within 130 revolutions and the maximum displacement occurs at 0.0097 s.

Discussion

Subbiah and Rieger [10] stated that the converging speed for the analysis of rotary systems is faster and is more accurate by using the Houbolt method than the Newmark method or the Wilson method. Therefore, the Houbolt method was used in this present combined methodology. The deviation between the calculated maximum transient displacements of the disk center and the data obtained by Subbiah and Rieger [10] decreases if N_C increases as shown in Table 2. The calculated time increases if N_C increases. Therefore, N_C equal to 30 is selected for further analyses.

The calculated computer times are not available in most of the studies. Alam and Nelson [11] utilized the computer program ARDS (Analysis of Rotor Dynamic Systems) for the analysis of rotary systems. However, neither Subbiah and Rieger [10] nor Alam and Nelson [11] mentioned the type of computers used and the calculated computer time in their studies. A personal computer, of which the calculated computer time is not available, was used in this study in order to reduce the cost of using computers. Since either various computers or various schemes of computer programs have different calculated computer times, comparisons for the calculated computer times are difficult to make. Although the calculated computer times for converging are not available, Fig. 7 shows the converging speed with N_C equal to 30 is faster for this present method than in the method used by Subbiah and Rieger [10]. Therefore, the calculated computer time should be shorter for this present method than in the method used by Subbiah and Rieger [10]. The deviation of the displacements may come from assumptions of the disk with the concentrated mass and the shaft without the mass made by Subbiah and Rieger [10]. Due to the nonisotropic bearings, the trace of the displacement is elliptical as shown in Fig. 8. Figure 9 shows that the transient displacements of the disk center are larger than those of the bearing center because the eccentricity of the disk is the source of vibration.

The calculated maximum transient displacements of the disk center for various rotational speeds of the shaft are closer to those obtained from using the software ANSYS of the finite element method than those obtained by Subbiah and Rieger [10] as shown in Fig. 10. Therefore, the accuracy of the calculated results is improved compared with the results obtained by Subbiah and Rieger [10]. The deviation of the calculated results from those obtained from using the software ANSYS may come from different numbers of elements used. The maximum deviations between the calculated results and those obtained by the software ANSYS and Subbiah and Rieger [10] are 2.86 percent and 5.37 percent, respectively.

For the second system, the critical speeds of the first mode, the second mode and the third mode of vibrations are 1550, 3100 and 4100 rad/s, respectively. These speeds are consistent with the results obtained by Alam and Nelson [11] as shown in Figs. 12, 13, 14 and 15. When the rotational speed of the shaft is less than 1550 rad/s, the maximum transient displacement of the disk center in the Y and Z directions are similar to those obtained by Alam and Nelson [11]. The deviations of the maximum transient displacements of the disk center in the Y and Z directions increase when the rotational speed of the shaft increases from 1550 to 4100 rad/s as shown in Figs. 12 and 13. The maximum transient displacements of the disk center in the Y and Z directions are larger than those obtained by Alam and Nelson [11] when the rotational speed of the shaft is faster than 4100 rad/s as shown in Figs. 12 and 13. For various rotational speeds of the shaft, the maximum steady displacements of the disk in the Y direction are similar to the data obtained by Alam and Nelson [11] as shown in Fig. 14. A comparison between the maximum steady displacements of the disk center in the Z direction and the data obtained by Alam and Nelson [11] indicates a maximum deviation of 3.45 percent when the rotational speed of the shaft is slower than 3700 rad/s. At the higher rotational speed of the shaft, the deviation is 6.07 percent. The maximum steady displacements of the disk center are 0.54 cm, 0.03 cm and 0.07 cm for the first mode, the second mode and the third mode of vibration, respectively.

When the rotational speed of the shaft is 1550 rad/s, a maximum displacement of 5.4 mm occurs at 0.2036 s in the steady state. When the rotational speed of the shaft is 3250 rad/s, a maximum displacement of 0.5 mm occurs at 0.0162 s in the transient state. When the rotational speed of the shaft is 4100 rad/s, a maximum displacement of 1.0 mm occurs at 0.0097 s in the transient state.

Conclusion

The results indicate that the maximum displacement may occur at the transient state due to the unbalanced effect, highlighting the importance of studying the dynamic behavior in the transient state. The selection of the time interval and the number of steps per revolution has an effect on the accuracy and the converging speed of the calculated result. Also, the converging speed of the numerical method depends on the system analyzed. This study shows that N_C between 25 and 35 can provide noteworthy results with a good converging speed by using the present method because it takes advantage of the individual methods used in this method. Therefore, the combined methodology in this study can provide calculated results with a faster converging speed and an improved accuracy.

Acknowledgment

The authors would like to thank the National Science Council of the Republic of China for the grant NSC88-2212-E-002-037 for funding this investigation and to Grant D. Huang for comments and revisions made on this manuscript.

Nomenclature

$[C]$ = damping coefficient matrix
c = damping coefficient
d = diameter
$\{F\}$ = external load
$\{F_D\}$ = unbalanced force acting on disk
$\{f\}$ = interaction force between elements
G = shear modulus
g = gravitational acceleration
I_D = diametral mass moment of inertia
I_p = mass polar moment of inertia
$[K]$ = stiffness matrix
k = stiffness
l = length
$[M]$ = mass matrix
m = mass per unit length
$\{\mathbf{q}\}$ = displacement vector
s = distance from left end of element to cross section
$[T]$ = transfer matrix
t = time
$\{\mathbf{u}\}$ = state vector
X,Y,Z = coordinates
y,z = translational displacement of center point in Y and Z directions
η_v = viscous damping coefficient
η_H = hysteretic loss factor
θ = rotational displacement in Y and Z directions
ϕ_k = rotational displacement function, $k=1,2,3,4$
ψ_j = translational displacement function, $j=1,2,3,4$
Ω = rotational speed of shaft

Subscripts

Downloaded 03 Nov 2008 to 140.112.113.225. Redistribution subject to ASME license or copyright; see http://www.asme.org/terms/Terms_Use.cfm

g = gravitation
i = sequence of time
n = nth element
T = translation
R = rotation
y = Y direction
z = Z direction

Superscripts

. = derivative with respect to t
b = bearing
d = disk
s = shaft
L = left end
R = right end
T = transverse matrix

References

[1] Adams, M., 1980, ''Nonlinear Dynamics of Multibearing Flexible Rotors,'' J. Sound Vib., **71**, No. 1, pp. 129–144.
[2] Nelson, H. D., 1980, ''A Finite Rotating Shaft Element Using Timoshenko Beam Theory,'' ASME J. Mech. Des., **102**, pp. 793–803.
[3] Dokainish, M. A., 1972, ''A New Approach for Plate Vibrations: Combination of Transfer Matrix and Finite-Element Technique,'' ASME J. Eng. Ind., **94**, pp. 526–530.
[4] Pestel, E. C., and Leckie, F. A., 1963, *Matrix Methods in Elastomechanics*, McGraw-Hill, New York.
[5] Kumar, A. S., and Sankar, T. S., 1986, ''A New Transfer Matrix Method for Response Analysis of Large Dynamic Systems,'' Comput. Struct., **23**, No. 4, pp. 545–552.
[6] Subbiah, R., Sankar, T. S., and Kumar, A. S., 1988, ''Transient Dynamic Analysis of Rotors Using the Combined Methodologies of Finite Elements and Transfer Matrix,'' ASME J. Appl. Mech., **55**, pp. 448–452.
[7] Nelson, H. D., and McVaugh, J. M., 1976, ''The Dynamics of Rotor Bearing Systems Using Finite Elements,'' ASME J. Eng. Ind., May, pp. 593–600.
[8] Houbolt, J. C., 1950, ''A Recurrence Matrix Solution for the Dynamic Response of Elastic Aircraft,'' J. Aeronaut. Sci., **17**, pp. 540–550.
[9] Özguven, N. H., and Özkan, L. N., 1984, ''Whirl Speeds and Unbalance Response of Multi-bearing Rotors Using Finite Elements,'' ASME J. Vib. Acoust. Stress Reliab. Des., **106**, pp. 72–79.
[10] Subbiah, R., and Rieger, N. F., 1988, ''On the Transient Analysis of Rotary Bearing Systems,'' ASME J. Vib. Acoust. Stress, Reliab. Des., **110**, pp. 515–520.
[11] Alam, M., and Nelson, H. D., 1985, ''A Blade Loss Response Spectrum for Flexible Rotor Systems,'' ASME J. Eng. Gas Turbines Power, **107**, pp. 187–204.
[12] Newmark, M. N., 1959, ''A Method of Computation for Structural Dynamics,'' ASME J. Eng. Mech. Div., **85**, pp. 67–94.
[13] Wilson, E. L., Farhoomand, I., and Bathe, K. J., 1973, ''Nonlinear Dynamic Analysis of Complex Structures,'' International Journ. of Earthquake Engineering And Structural Dynamics, **1**, pp. 241–252.
[14] Bathe, K. J., and Wilson, E. L., 1976, *Numerical Methods in Finite Element Analysis*, Prentice Hall, Englewood Cliffs, New Jersey.

Downloaded 03 Nov 2008 to 140.112.113.225. Redistribution subject to ASME license or copyright; see http://www.asme.org/terms/Terms_Use.cfm